Optimisation and Modelling of the Wear Properties of Laser-Coated SiC-Blend Ni Welds on Steel Substrates

Dezheng WU [1], Canyu DING [2], MingDer JEAN [1]*

[1] *College of Arts and Design, Jimei University, 185 Yinjiang Rd., Jimei District, Xiamen 361021, China*
[2] *Xiamen City University, Qianpu South Road, Siming District, Xiamen 361000, China*

http://doi.org/10.5755/j02.ms.37320

Received 21 May 2024; accepted 9 July 2024

In the present work, a ceramic-metal matrix composite coating with the optimization and modelling of mechanical properties of Ni added SiC powders was studied on 45 steel by laser cladding. An artificial intelligent approach, which uses adaptive network fuzzy inference systems (ANFIS) based on experimental designs, is used to model the tribological behaviour of welds. An orthogonal array experiment is used and the effect of the deposition parameters on the welds is determined. Based on the average analysis and analysis of variance (ANOVA), four important factors are taken as inputs for the fuzzy logic inferences, while the loss of wear was taken as the output of the ANFIS. The welds are analysed using scanning electron microscopy (SEM) and wear tests are performed, using a pin-on-disk tribometer. This study identifies a group of highly developed needle-like dendrites and finer eutectic crystals, and lower wear volume loss is evident in the Ni-SiC welds. The ANFIS model based on Taguchi's design provides a better response pattern which shows extremely good fitting. As a result, satisfactory results are obtained between the predicted and experimental values of wear on laser coated Ni-added SiC welds, thereby validating the reliability and feasibility of this method.
Keywords: silicon carbide, ANFIS neural network, wear properties, metal matrix composite and laser cladding.

1. INTRODUCTION

Available in industrial applications, metal matrix composites in the form of coatings for hard surface environments with protective powers against high temperature, wear, corrosion, impact and fatigue, are of much attention, especially in the fields of cutting tools, turbine blades, engine valves, and so on. Recently, there has been a great deal of interest in the use of ceramic matrix composites including carbides, nitrides and borides on steel and non-ferrous alloys, because of their integrated properties, which have proved to be an excellent protective material in additive manufacturing [1, 2]. These carbides can effectively improve the wear resistance of metal matrix composites. Silicon carbide alloys possess a high melting point (2500 °C) and hardness (2700 kgf/mm^2), which are of importance for sandpaper, grinding wheels and cutting tools, which has long been used by manufacturers for equipment such as bearings in high-temperature environments, heated mechanical parts, automotive brakes and even knife-sharpening tools [3 – 6]. In addition, silicon carbide possesses a unique combination of properties such as excellent oxidation resistance, high- temperature strength retention, high wear resistance, high thermal conductivity, good thermal shock resistance and, above all, elastic resistance at temperatures up to 1650 °C making it very versatile, which are commonly used in areas such as electric vehicles, solar energy systems and data centres due to their low cost, high voltage demands with prowess, abrasion and corrosion resistance. Therefore, it is recognised as an important structural ceramic material.

Silicon carbide alloys have high wear and corrosion resistance and are therefore widely used in severe environments such as high temperatures, abrasion, corrosion, impact, and fatigue [7 – 9]. It has a promising potential to be applied in the manufacture of metal-ceramic composite coatings by laser cladding. Whereas, it is difficult for typical silicon carbide alloys to meet the requirements of workpieces in harsh operating environments due to the high melting point of silicon carbide alloys, which makes them susceptible to porosity or cracking in the liquid state, as well as their high hardness and brittleness, which makes them difficult to machine. Moreover, a series of drawbacks of cemented carbides have been noticed, including diminished strengthening, non-uniform distribution, thermal stress concentration and crack formation, especially in high volume fraction cemented carbide coatings, thereby limiting the application of cemented carbides [10 – 13]. Facing some of these challenges, various kinds of surface modification techniques, including composite coatings with transition metals, have been investigated due to their good wettability and ductility. There is a requirement to extend some useful self-melting alloys to high carbide silicon carbide to improve the properties of silicon carbide composites through further in-depth exploration. Recently, several researchers have worked on developing different methods to improve the performance of high carbide coatings [14 – 16]. These methods are designed to eliminate some of the defects in the weld, such as preheating the base material, functionally graded coatings, the addition of self-melting alloy and laser-induced hybrid welding. Available publications have addressed the use of metal matrix composites with self-melting alloys for the manufacture of metal-ceramic coatings by laser cladding [17 – 19]. These

* Corresponding author. Tel.: +0592-6181815; fax: +0592-6180809.
E-mail: *202261000183@jmu.edu.cn* (M.D. Jean)

powders possess a binder phase that protects the carbide against oxidation and decomposition [20 – 21]. They are usually formed by adding transition metals as binder phase materials to brittle carbides to form metal-ceramic composites, thus reducing structural defects in highly brittle carbides during laser cladding. Based on the above literature, many studies have shown that metal matrix composites with binder phase additives in highly wear- and corrosion-resistant environments have the potential to improve the susceptibility problem of ceramic reinforced coatings during laser cladding, and these results have been successfully applied by industry. However, the laser cladding process is a highly nonlinear, multivariate, strongly coupled and complex process with a large number of stochastic uncertainties, where decisions often need to be made based on experience, but without good results [22]. It is highly difficult to control the effect of mechanical properties of metal-ceramic composite deposits under the combination of multiple parameters, using trial and error methods. Thus, in order to control the mechanical properties of metal-ceramic composites that are made by laser cladding, several new attempts are needed.

Methods such as response surface methodology, artificial neural networks, and fuzzy inference systems are utilized most popularly for manufacturing process modelling. Yet, constructing appropriate fuzzy membership functions and fuzzy rules is indeed a difficult and time-consuming task. Therefore, a method that employs the integration of both neural networks and fuzzy logic is needed, because of their ability to produce adaptive predictions, models complex processes using a small amount of data in a short period of time. Although the optimisation of metal-ceramic composites applied to the welding process has been reported in the literature, the study of optimising the performance of nickel-doped silicon carbide by laser cladding using adaptive network fuzzy inference systems (ANFIS) in Taguchi's method is seemingly yet to be reported.

In this study, an ANFIS neural network algorithm based on Taguchi's experiments is established through the identification of suitable combinations of control factors that improve the wear performance of laser-coated silicon carbide welds. A model of the wear performance of laser-clad Ni/SiC welds by parameter combinations is established. This experiment allows us to understand the effect of various variables on Ni-SiC welds and to simulate the tribological behavior of welds by laser cladding in order to obtain better wear quality. It not only evaluates the effect of the parameters on the response, but also optimizes the parameters so that the tribological properties of the laser-coated weld can be better understood.

2. EXPERIMENTAL DESIGN AND ANALYSIS

2.1. Materials and preparations

The laser cladding equipment used in this test is composed of YLS-3000 fiber laser, a six-axis robotic arm, a laser water cooler and a PLC control system as shown in Fig. 1 a. In addition, the laser cladding experiments use axial nozzles in Fig.1b, which utilizes nitrogen to carry the cladding powder from the feeder to the melt pool, thereby generating protective welds during the process of deposits. It uses an IPG YLS-3000 fiber laser with a maximum power of 3000 W and a wavelength of 1.07 μm. Nickel alloy powders are applied into silicon carbides that formed metal-ceramic composite welds in order to improve the properties of the highly hardened silicon carbide. The microstructure of the nickel-added silicon carbide deposits is examined using a scanning electronic microscope and energy dispersive spectrometry (Hitachi S-2600H, Tokyo, Japan). In the wear test, the surface of the weld material is tested for wear resistance by performing a reciprocating wear test using a UMT-2 scratcher. The wear volume is calculated by measuring the trajectory area of each contact surface with a 3D surface profiler, which is used in conjunction with a scanning electronic microscope that observes the surface.

a b

Fig. 1. a – laser cladding equipment used in this test; b – a schematic picture of the laser cladding process

2.2. Experimental design and layout

With laser cladding, a number of controlled variables are required to minimize unwanted defects in the weld. Therefore, the variables of laser cladding must be controlled. Table 1 shows the control factors and the level of each factor in the Taguchi design, where six 3-level factors containing A, B, C, D, E, and F were allocated to the orthogonal arrays. These factors and their alternative levels that were used in the experiment are listed in the orthogonal array (3^6). In order to evaluate the influence of factors on the response, Taguchi suggests using a special form of response transformation called signal-to-noise ratio (S/N), which measures quality with emphasis on variation [11].

Table 1. The control factors and levels of the Ni ratios for the SiC mixtures in this study

Level	Ratio of powder, %	Preheat temperature, ℃	Laser power, W	Carrier gas flowrate, mL/min	Scanning speed, mm/s	Stand-off distance, mm
1	100%SiC+0%Ni	25	1000	1400	2	15
2	90%SiC+10%Ni	100	1400	1600	4	20
3	80%SiC+20%Ni	200	1800	1800	6	25

The S/N ratio based on the loss functions is calculated from Eq. 1:

$$S/N_i = -10\mathrm{Log}\sum_{i=1}^{n}[(\bar{y}_i - m)^2 + S_i^2], \quad (1)$$

where $\bar{y}_i$ is the mean and *Si* is the standard deviation of the i^{th} trial, *m* is the predefined value of 18 triails, which is measured in decibels. The S/N ratio was calculated, and the mean and standard deviation of each variable are summarized in Fig. 3. Each trial was repeated three times for wear volume, which was analyzed for rank order and maximal values using mean value analysis with the S/N ratio, analysis of variance (ANOVA) was also used again to determine the significant factors for each quality characteristic. Subsequently, predictions of quality characteristics were made using these factors incorporated into the ANFIS model.

2.3. Adaptive network based fuzzy inference system

An adaptive neuro-fuzzy inference system (ANFIS)is a hybrid predictive model that uses both neural networks and fuzzy logic, which is a method for generating mapping relationships between inputs and outputs. The structure of the model consists of five layers, where each layer consists of several nodes. As with neural networks, the inputs to each layer in the ANFIS structure are obtained from the nodes in the previous layer. Fig. 2 depicts the architecture of ANFIS. It is deduced from Fig. 2 that the network consists of m inputs (X_1, ..., X_m), where each input is organized by n membership functions. In addition, the layer containing R fuzzy rules and the output layer are useful at building the model. The number of nodes in the first layer can be calculated as the product of m (number of inputs) and n (number of fuzzy functions) (N = m·n). The number of nodes in the other layers (layers 2 – 4) is linked to the number of fuzzy rules (R). Fig. 2 shows the topology of the proposed ANFIS for wear volume loss. For more details on the implementation of the ANFIS network, it is referred to the literature [13]. ANFIS uses membership functions for several sets while employing the linear functions of the Sugeno type for the rule output. Various types of membership functions (MF) are used, such as triangular, trapezoidal, gaussian, and bell functions. The architecture of the neuro-fuzzy model consists of five unique adaptive layers. Takagi and the Sugeno proposed the T-S fuzzy model in 1985. The model was later called Sugeno fuzzy model. It is a nonlinear model that expresses the dynamic properties of complex systems and is the most commonly used fuzzy inference model. An example of a simple fuzzy inference system, is a first-order model of fuzzy Sugeno that is a typical rule base, which contains two If-then rules can be expressed as follows:

Rule R_{ij}: if x_1 is A_{11}, x_2 is A_{12}, …, and x_n is A_{nj};

then $y_j = f(x_1, x_2, \ldots, x_n)$ $i = 1, 2, \ldots, n$; $j = 1, 2, \ldots, k$, (2)

where x_i is the antecedent input, A_{ij} is themembership function and $f(x_1, x_2, \ldots, x_n)$ represents the outputs in the consequent part. Typically $y_j = f(x_1, x_2, \ldots, x_n)$ is a constant or linear. The following is a brief description of the Sugeno first-order model with two input variables.

Layer 1: The input X_i is fuzzified by the membership function that is transformed to obtain the membership degree of the linguistic type A_{ij} (e.g., large, medium, small) in the interval [0,1]. The output, O_{ij}, of this layer can be expressed as

$$O_{i1} = \mu_{ij}(X_i),\ i = 1, 2, ..., n,\ j = 1, 2, ..., m, \quad (3)$$

where μ_{ij} is the j^{th} membership function for the input X_i.

Layer 2: The firing strength of each rule is obtained by multiplying the degrees of membership of each rule;

Layer 3: The trigger strength of each rule obtained by the previous layer is normalized to characterize the trigger weight of the rule in the whole rule base;

Layer 4: Calculated results of a linear combination of input functions using normalized weights(w);

Layer 5: The output of the calculation is the sum of the results of the linear combination of the normalized weights $(\bar{w}_i)$ of each rule.

$$O_{i5} = \sum_{i=1}^{n} \bar{w}_i f_i(x_{1,}x_{2,\ldots,}x_{n)}. \quad (4)$$

In this paper, in order to make the training more stable, the parameters in the model are divided into the premise and consequent parameters, which are learned by a mixture of the backpropagation algorithm and the least squares method. The least squares estimation of the consequent parameter is performed in the forward propagation process, whereas only the premise parameter is updated in the backpropagation process. The total number of experimental data used to generate the ANFIS model was 36. In this study, 21 training data and 15 test data were used.

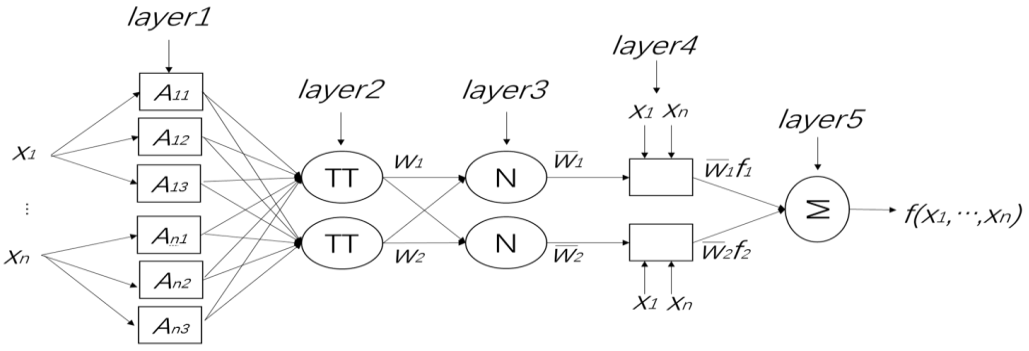

Fig. 2. A framework of ANFIS model with five layers including a fuzzy layer, a rule-based layer, a normalization layer, an inference layer and an output layer

The Root Mean Square Error (RMSE) function is applied to this network to check the performance of the trained model.

It is calculated using the following formula:

$$O_{i5} = \sum_{i=1}^{n} \overline{w}_i \, f_i(x_{1,}x_{2,\ldots,}x_n) \,, \quad (5)$$

where m is the total number of training sample, di is the real output value, and y_i is the ANFIS output value in training algorithms.

3. EXPERIMENTAL RESULTS AND DISCUSSION

3.1. Experimental analysis based on orthogonal array

Fig. 3 shows the results of the L18 experiments in which the wear resistance of the welds with nickel added to silicon carbide was evaluated for each experimental test by calculating the S/N ratio from the experimental values and standard deviations. The experimental results show that there is a great difference in wear resistance compared to the substrate with an increase of about 4 times, while the wear volume loss in the wear test is reduced accordingly, which indicates good wear resistance. In trials 4, 5, 14 and 17, wear volume exceeded 90×10^{-5}mm^3, i.e. the lower the S/N ratio, the more it indicates heavier wear, while in trials 2, 6, 15 and 18, wear volume is lower than 40×10^{-5}mm^3, i.e. the higher the S/N ratio, the more it indicates smaller wear.

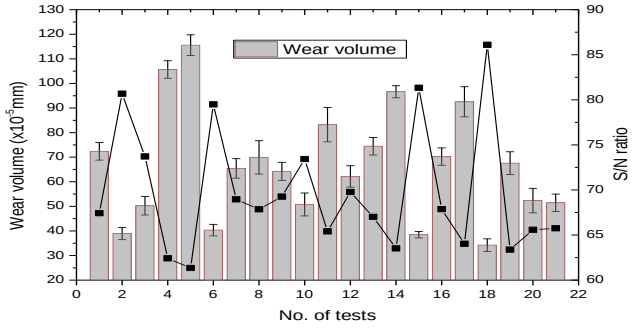

Fig. 3. Comparison of signal-to-noise ratio and wear volume with a standard deviation of nickel-added silicon carbide welds by laser cladding

3.2. Microstructure of the weld zone of laser cladding

The SEM micrographs of the cladding weld are shown in Fig. 4, where the microstructures of the Ni added SiC grains can be visualised, while the chemical compositions of Ni doped SiC welds obtained by EDS are given in Table 2. Due to the different contents of nickel in the silicon carbide in the molten pool during the laser cladding process, different forms of carbides and precipitates are induced in the composite coatings. The EDS results for the typical regions that were marked with trials 2, 7, 13, and 17 are shown in Fig. 4. As shown in the left-upper zone of Fig. 4, there is a cladding zone, a heat-affected zone, and a substrate in the cross-section of the deposits, respectively. The micrographs in Fig. 4 further show that the dendritic protrusions melt zone is much coarser near the interface between the melt zone and the heat affected zone. In addition, it can be observed that the fine dendritic patterns are denser near the boundary of the crystalline grains. The cladding zone is a grey zone and the heat affected zone is a bright grain zone. Fig. 4 a shows that the interface between the molten zone and the substrate is found to be well adherent and free from defects. There are some grey areas in the weld zone containing small dendritic crystals and fine microstructures, while the white areas have irregular needle-like structures, some pits and less crack. Black graphite, pores, cracks, roughness and surface irregularities are evident in the cross-section cladding zone shown in the left-upper zone of Fig. 4 b. The thickness of the melt layer is about $3-5$ microns, which is much less than that produced by the other fractions. As shown in the magnified view of Fig. 4 b, the melting zone of the laser cladding contains irregular unmelted SiC particles and a large number of eutectic nanocarbides at trial 7. In addition, the white areas of the melting zone show blocks of unmelted Si- and C-type phases with fine grains growing around them, while the light-colored areas show the formation of eutectic crystals enriched with Fe, Ni, and O phases. Unfortunately, the partial dissolution of SiC on the melt could not be avoided in this study. This is due to the difference in the temperature gradient of the melt pool between the white and dark zones, which affects the subsequent solidification and the corresponding structure during the deposition of the cladding. By comparing Table 2 and Fig. 4, it can be seen that Fig. 4 b contains more Si and C elements while less O than Fig. 4 a in the EDX analysis of the laser cladding. This can also be observed from the SEM observations that the different structures of carbides containing undissolved silicon carbide particles, precipitates, dendrites, blocks, grains and graphite are almost randomly distributed in the melt pool. As shown in Fig. 4 c, the grain growth was incomplete, where eutectic grains could be seen along the grain boundaries, as shown in the upper part of the SEM micrograph. A typical area labelled Test 13 in Fig. 4 c is shown in Table 2 with EDS results. The elemental distribution of the melting zone by X-ray diffraction shows white areas rich in C and Fe while less O, Si and Ni, which are dominated by silicon carbides (SiC), iron carbides (FeC_3) and iron silicides (Fe_2Si) [9]. As shown in Fig. 4 d, most of the molten zones containing cloud-shaped grey clusters of Fe and coarse particles of fused SiC can be clearly seen in the cladding layers. The analysis of test 17 by EDS is shown in Table 2.

Table 2. The chemical composition of silicon carbide with nickel additives by wt.% of atomic concentration as shown by EDS surface analysis in Fig. 4

No. of trials	Atomic concentration, %				
	C	O	Si	Fe	Ni
Trial 2	20.2	37.5	0.41	41.9	0.00
Trial 6	18.9	35.9	0.09	45.1	0.00
Trial 13	0.00	82.8	0.70	16.4	0.00
Trial 17	0.00	28.5	0.13	71.4	0.00

Coarsened carbides are found in the white areas, while Fe, O, and Ni phases are visible in the darker areas. The decrease of carbon to 88.655 % and the increase of O and Fe by more than a factor of 4 in the molten areas indicate that most of the SiC base has melted in the white area. As mentioned above, the SiC particles have been fully dissolved in the cladding zone, where the initial precipitation of carbides is detected in the white areas and

many finer Fe- and Si-based phases in darker areas. Uneven distribution is observed throughout the melting zone. On the other hand, the grains of silicon carbide are completely melted without any defects in the SEM micrographs. These results are not good for anti-wear.

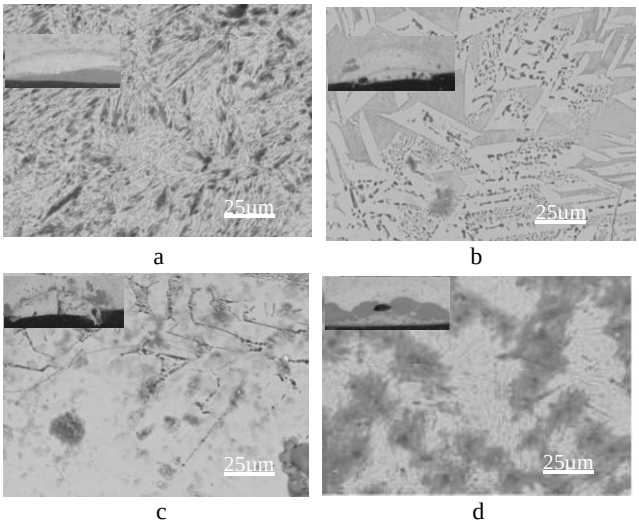

a b c d

Fig. 4. SEM microstructures and coating profiles of various tests in the cladding deposits (small image at the top left of the SEM) containing the melt zone, the heat affected zone and the substrate: a – test 2; b – test 7; c – test 13; d – test 17

3. 3. Wear properties of Ni mixed SiC deposits

The results of the tests on the worn volume of various coatings are given in Fig. 3, where various patterns and EDS analysis of wear can be visualised. The distribution of wear volume was 32.65×10^{-5} mm^3, 65.43×10^{-5} mm^3, 80.35×10^{-5} mm^3 and 117.84×10^{-5} mm^3 in Trial 2, Trial 7, Trial 13 and Trial 17 respectively, which indicates that they are significantly lower than that of the substrate. As can be seen in the upper-right plot of Fig. 5, the integral method is applied to the areas of wear tracks on each cross-section, where wear is more serious in the blue areas while less in the red areas. Fig. 5 a shows a three-dimensional topographic profile of the wear track of the Test 2 sample, as well as a photograph of the two-dimensional profile for wear. It has minimal wear volume in the orthogonal array. The 2D topography of the corresponding wear scars on the wear surface shows deep grooves with smooth, broad continuous trajectories, reflecting a wear depth of 1.75um. In addition, the EDS analysis shown in Table 3 indicates that the wear surface is rich in C, O and Fe as well as a small amount of Si. Obviously, hard silicon carbide and its tungsten carbide counterpart are easily prone to form wear barriers when they wear against each other. This is mainly due to the high carbide hardness caused by the abrasion mechanism.

Table 3. The distribution of the EDS spectrum of worn patterns with test 2, test 7, test13 and test17 from the track for welded joints.

No. of trials	Atomic concentration, %				
	C	O	Si	Fe	Ni
Trial 2	94.3	0.21	0.01	5.38	0.05
Trial 7	96.0	0.02	0.16	3.74	0.09
Trial 13	96.2	0.19	0.18	3.41	0.00
Trial 17	88.7	0.91	0.01	20.4	0.07

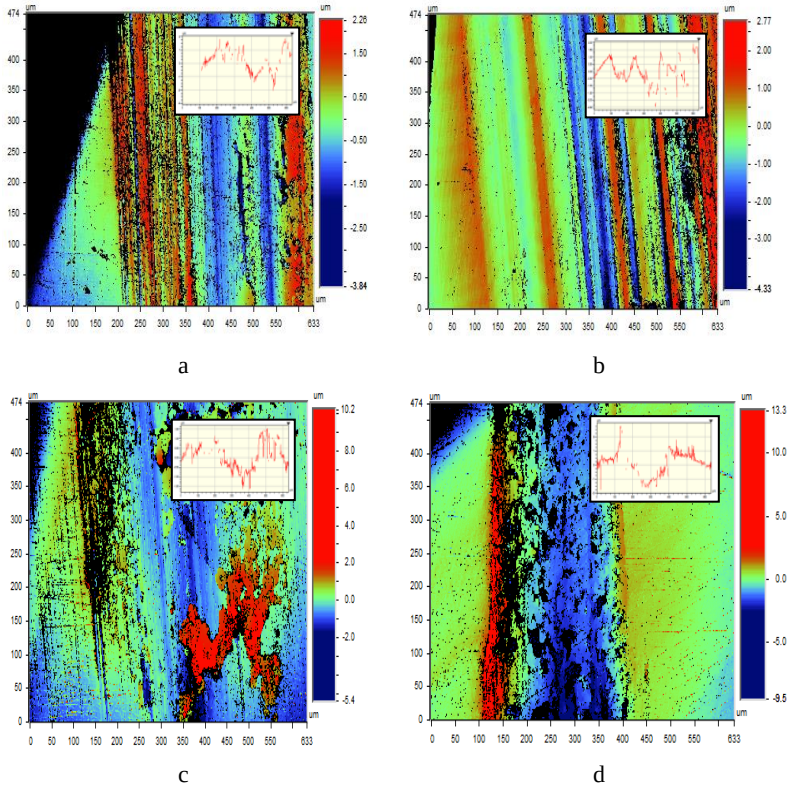

a b c d

Fig. 5. The 3-D topographs of the wear track by wear test with the cross-sectional profile included: a – trial 2; b – trial 7; c – trial 13; d – trial 17 for cladding welds

Therefore, these coatings are protected by the carbides which are difficult to remove after wear. Similarly, in the case of test 6, the wear mechanism of the worn surface is close to that of test 7. As shown in Fig. 5 b, the worn surface is covered with a number of uneven pits with abrasion marks that are 2.75 μm deep. Some of the light green areas showed less deformation and fewer transferred fragments, which suggested the presence of a wear mechanism. Furthermore, the results of the EDS analysis shown in Fig. 5 b are given in Table 3. Compared to Fig. 5 a, the wear surfaces have lower C and O contents while the Fe content is higher. There are several noticeable bands of plastic deformation in the area of adhesive. The wear zone is characterized by the presence of a higher amount of Fe in the austenitic dendrites. This situation leads to several bands of marked plastic deformation, which become sensitive to wear. Hence, it is hardly expected that the wear resistance in this region can be improved. Compared to Fig. 5a, Fig. 5 b shows deeper grooves on the wear surface with several smooth, extensive, and continuous tracks, reflecting more than four times the amount of wear. The wear surface shows greater areas of plastic deformation (blue) and very few traces of wear debris (red) under test13 as shown in Fig. 5 c. This shows significant signs of adhesive wear and severe plastic deformation. Similarly, there is also evidence from the EDS analysis results shown in Table 3 that the wear surface is rich in O and Fe with small amounts of Si. More wear damage can be seen in Fig. 5 d. In addition, the results of the EDS analysis shown in Table 3 indicate that the wear surface is enriched with O and Fe, while Fe is nearly three times as much as O atoms. Apparently, the iron fragments of the substrate contacted by the corresponding parts were carried into the wear track. The blue-colored area shows higher Fe content, where metal oxide film is formed during the sliding process. The main reason for this phenomenon is that the coating is damaged by its high hardness counterpart during wear, resulting in the wear surface containing a large amount of iron, which proves that the coating is no longer able to protect the substrate. The EDS analyses shown in Table 3 indicate that the wear surfaces do not contain C and Ni. It is clear that the hard surfaces of hard silicon carbide and tungsten carbide are unable to form wear barriers when they wear against each other. Accordingly, the C and Ni bonded carbides are detached from the coatings. That is, there is too much iron in Fig. 5 c and d on the worn surface that the coating cannot withstand much wear. Consequently, wear resistance cannot be improved. However, with the increase in wear volume, adhesive wear becomes more significant than abrasive wear. The wear resistance of laser welded joints is significantly improved due to the high amount of carbides in the weld.

3.4. Effect of Ni additive mixed SiC on wear properties

The effects of mean values can reflect the importance of the relative performance between each of the control factorial levels. The S/N was applied according to Eq. 1 in Fig. 6, and the average response and ranking of effects in the experimental results were evaluated. The ranking of factorial effects in Fig. 6 further shows that factors C, D, E and F strongly influence wear variability, whereas A and B are less influential. As seen in Fig. 6, A3, B1, C3, D2, E1 and F2 have the largest values with the greatest impact on the amount of wear. i.e., they are the optimum values. Furthermore, a further analysis of variance was done in Table 4 to validate the significance of the control factors in Fig. 6. Table 4 shows the mean square of the six control factors, which illustrate the relative impact of the factors on reducing variation. In this study, Based on AVOVA, we chose laser power (C), carrier gas flow rate (D) scanning speed (E), and spacing (F) to be of great importance, whereas nickel added SiC content (A), and preheating temperature (B) were less important, as shown in Table 4. We again recognize the most important factors obtained from the average factor analysis. They were identified to be further incorporated into the predictors of the ANFIS for the worn volume losses of the weld by laser cladding.

Table 4. An ANOVA table for S/N ratios during the worn volume losses of welds by laser cladding

Control factors	Sum of squares	Degrees of freedom	Mean square
A	20.138	2.0	10.069
B	19.702	2.0	9.851
C	334.066	2.0	167.033
D	49.774	2.0	24.887
E	51.961	2.0	25.981
F	37.953	2.0	18.977
Error	356.281	41.0	8.690
Total	869.876	53.0	16.413

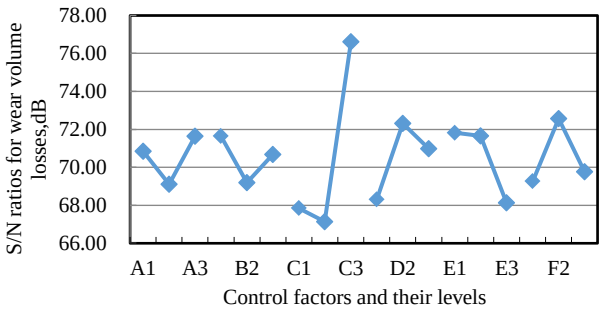

Fig. 6. The main effect for S/N ratios during the wear volume of welds by laser cladding

3.5. Factorial effects and their optimization based on wear behaviors

To estimate the optimal performance of the welds used in the tests, each test was repeated three times in different areas of the worn tracks. Fig. 2 shows the results and S/N ratios using formulas that satisfy the smaller-is-better property. The optimal setting for the factorial levels is $A_3B_1C_3D_2E_1F_2$. That is, the optimal parameters are determined in accordance with the effect of the S/N ratio, so the Ni doped SiC welds can be clearly distinguished. The optimal parameters for the sputtering process are: a ratio of powder of 80%SiC +20%Ni, a preheat temperature of 25 °C, a laser power of 1800 W, a flowrate of carrier gas of 1600 mL/min, a scanning speed of 2 mm/s, and a stand-off distance of 20 mm. In all 18 sets of orthogonal array experiments, we selected 4 sets with well distributed results such as sets 2, 7, 13 and 17 in comparison with the optimal parameters. The lower the wear resistance, the closer it is to

the left side of the graph, as shown in Fig. 7. Using a Gaussian plot, the finest bold solid curve shown on the left side of Fig. 7 indicates the best test, which produces the smallest wear volume loss with only a small deviation. It is evident that the optimal settings of the control factors are significantly resistance to variability, which indicates good reproducibility.

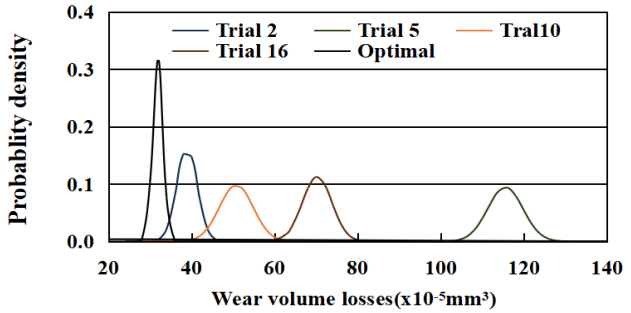

Fig. 7. Comparison of probability density for the five trials in the orthogonal table with trial 2, trial 7, trial 13, trial 17 and the optimal trial

3.6. Predictive results of ANFIS models

To understand the performance of ANFIS, the significant parameters such as laser power, the flowrate of carrier gas, scanning speed and stand-off distance of Ni additive mixed SiC on wear volume loss by laser cladding are listed in Table 4, which are allocated to the adaptive network based fuzzy system. An adaptive neuro-fuzzy inference system was used to forecast the loss of wear volume. For this purpose, the MATLAB R2021 software package was used. In this paper, first-order TSK-type fuzzy rules are used to create predictive models. Different number of membership functions were tested using the subtractive clustering method to find the most accurate model. However, triangular types of membership functions were optimally applied. As shown in Fig. 2, the fuzzy logic system trained by a neural network has a rule base with 4 inputs and 1 output. This model can be used to predict the wear volume of Ni added SiC welds by laser cladding. For example, the four inputs are 1400 W, 1600 mL/min, 4 mm/s and 20 mm, respectively, whilst the predicted value is 38.9×10^{-5} mm3. A fuzzy layer, a rule base layer, a normalisation layer, an inference layer and a total output layer are optimally yielded. The wear response in the training and test datum of the ANFIS model yielded the following structure, where the 21 membership functions had the RMSE values of 0.061 and 0.063, respectively, using a subtractive clustering method. The performance of the model is validated by the RMSE. As shown in Fig. 8, the distribution points of the outputs of the training algorithms. Red dots are predicted values and blue dots are experimental data. The predicted and experimental values are very close to each other, indicating that the model is reliable. In addition, the ANFIS predictor also fits the distribution curve of the actual data. The ANFIS predictor fits the distribution curve of the actual data, where significant factors are incorporated into ANFIS. Many of the validation tests had an error of less than 3%, with a maximum error of 9.47 %. There is however a stable fluctuation in the distribution of prediction errors for ANFIS, with only two of the prediction errors exceeding the standard deviation of the experimental values by more than 5 %. A comparison of the experimental data with the ANFIS predictions is shown in Fig. 9 with testing algorithms., where the ANFIS predictor produced an average error of 3.98 %. As a result, the developed ANFIS model is an effective model for decision makers when analysing the tribological properties of nickel doped silicon carbide welds.

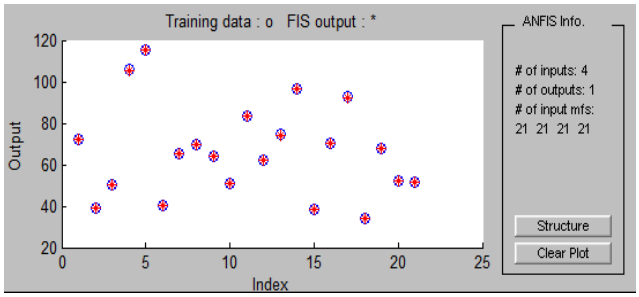

Fig. 8. The distribution points of the output of the training algorithms

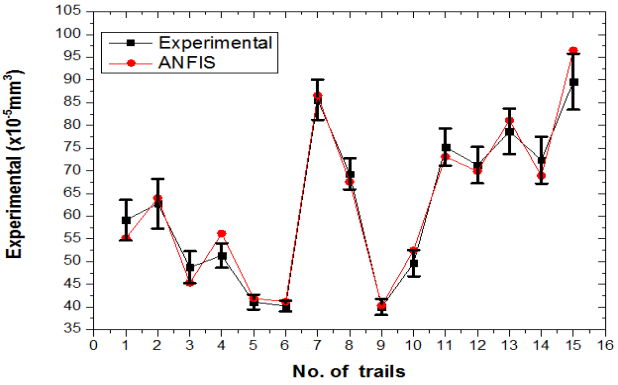

Fig. 9. Comparison of ANFIS model predictions with red dots and experimental data with black dots with testing algorithms

4. CONCLUSIONS

In this study, ceramic-metal based composite coatings were investigated on 45 steel by laser cladding which optimized the wear properties of nickel additives in silicon carbide welds. The difference in wear resistance compared to the substrate is significant, increasing by approx. 4 times, while the corresponding reduction in the wear volume loss during the wear test indicates good wear resistance. The microstructure of the melting zone is mostly in the form of fine dendrites, with grey areas in the melting zone that are more densely populated near the grain boundaries, while heat-affected zones are brightly grained. Besides, the results of EDS analysis of the worn areas show that the worn surfaces have lower C and O contents and higher Fe content. There is a more obvious plastic deformation zone in the cladding zone. In addition, the relationship between the significant parameters and the volume of wear by laser cladding was constructed using ANFIS. The wear response structure of the ANFIS model training and test data, where the 21 membership functions have the RMSE values of 0.061 and 0.063, respectively. It is clear that in ANFIS, the predicted and observed values are very close to each other, which indicates that the model has good predictive ability within the experimental domain. Overall, ANFIS provides

more reliable modelling of the cladding process, which verifies that the Ni added SiC welds by laser cladding are reliable and feasible.

REFERENCES

1. **Suryanarayanan, R.** Plasma Spraying: Theory and Aapplications. World Scientific. 1993.
2. **Sun, G., Zhou, R., Lu, J., Mazumder, J.** Evaluation of Defect Density, Microstructure, Residual Stress, Elastic Modulus, Hardness and Strength of Laser-Deposited AISI 4340 Steel *Acta Materialia* 84 2015: pp. 172 – 189. https://doi.org/10.1016/j.actamat.2014.09.028
3. **Ross, P.J.** Taguchi Techniques for Quality Engineering, 2nd edn., McGraw-Hill, New York, 1995.
4. **Da, S., Zhu, G.L., Zhang, K., Yao, C.W., Li, D.Y., Dai, Z.B.** In situ Synthesized High Volume Fraction WC Reinforced Ni-Based Coating by Laser Cladding *Materials Letters* 195 2017: pp. 178 – 181. https://doi.org/10.1016/j.matlet.2017.02.076
5. **Contin, A., de Vasconcelos, G., Barquete, D.M., Campos, R.A., Trava-Airoldi, V.J., Corat, E.J.** Laser Cladding of SiC Multilayers for Diamond Deposition on Steel Substrates *Diamond & Related Materials* 65 2016: pp. 105 – 114. https://doi.org/10.1016/j.diamond.2016.02.007
6. **Zhuang, H., Zhang, L., Staedler, T., Jiang, X.** Nanoscale Integration of SiC/SiO2 Core-Shell Nanocables in Diamond through a Simultaneous Hybrid Structure Fabrication *Applied Physics Letters* 100 2012: pp. 193102. http://dx.doi.org/10.1063/1.4712044
7. **Kumar, A., Das, A.K.** Evolution of Microstructure and Mechanical Properties of Co-SiC Tungsten Inert Gas Cladded Coating on 304 Stainless Steel *Engineering Science and Technology* 24 2021: pp. 591 – 604. https://doi.org/ 10.1016/j.jestch.2020.10.001
8. **Kumar, A., Ram, R.K., Das, A.K.** Mechanical Characteristics of Ti-SiC Metal Matrix Composite Coating on AISI 304 Steel by Gas Tungsten Arc (GTA) Coating Process *Materials Today: Proceedings* 17 2019: pp. 111 – 117. https://doi.org/10.1016/j.matpr. 2019.06.407
9. **Li, Q., Song, G.M., Zhang, Y.Z., Lei, T.C., Chen, W.Z.** Microstructure and Dry Sliding Wear Behavior of Laser Clad Ni-Based Alloy Coating with the Addition of SiC *Wear* 254 2003: pp. 222 – 229. http://dx.doi.org/10.1016/S0043-1648(03)00007-3
10. **Majumdar, J.D., Chandra, B.R., Nath, A.K., Manna, I.** Laser Composite Surfacing of Stainless Steel with SiC *Physica Status Solidi* 203 (9) 2006: pp. 2260 – 2265. https://doi.org/10.1002/pssa.200566021
11. **Myers, R.H., Montgomery, D.C., Anderson-Cook, C.M.** Response Surface Methodology: Process and Product Optimization Using Designed Experiments. 3rd ed, John Wiley & Sons, Inc., Hoboken, New Jersey. 2009.
12. **Li, N., Xiong, Y., Xiong, H.P., Shi, G.Q., Blackburn, J., Liu, W., Qin, R.Y.** Microstructure, Formation Mechanism and Property Characterization of Ti+SiC Laser Cladded Coatings on Ti6Al4V Alloy *Materials Characterization* 148 2019: pp. 43 – 51. https://doi.org/10.1016/j.matchar.2018.11.032
13. **Jang, J.S.R.** ANFIS: Adaptive-Network–Based Fuzzy Inference System *IEEE Transactions on Systems, Man, and Cybernetics* 23 1993: pp. 665 – 685. https://doi.org/10.1109/21.256541
14. **Pal, S., Pal, S.K., Samantaray, A.K.** Artificial Neural Network Modelling of Weld Joint Strength Prediction of a Pulsed Metal Inert Gas Welding Process using Arc Signals *Journal of Materials Processing Technology* 202 2008: pp. 464 – 474. https://doi.org/10.1016/j.jmatprotec.2007.09.039
15. **Zhang, C.Y., Chen, S.Y., Yang, E., Jean, M.D.** Effect of Cobalt Fraction Mixing WC Clads on Microstructural Evolution, Crack Formation and Tribological Properties by Laser Cladding *Journal of Physics: Conference Series* 2519 2023: pp. 012039. http://dx.doi.org/10.1088/1742-6596/2519/1/012039
16. **Contuzzi, N., Casalino, G.** On Modelling Nd:Yag Nanosecond Laser Milling Process by Neural Network and Multi Response Prediction Methods *International Journal for Light and Electron Optic*s 284 2023: pp. 170937. https://doi.org/10.1016/j.ijleo.2023.170937
17. **Liu, M., Duan, C.Z., Li, G.H., Cai, Y.J., Wang, F., Li, L.** Multi-response Optimization of Ni-based Laser Cladding via Principal Component Analysis and Grey Relational Analysis. Optik-International *Journal for Light and Electron Optics* 287 2023: pp. 171122. https://doi.org/10.1016/j.ijleo.2023.171122
18. **Zhou, Z.J., Du, Y.B., He, G.H., Xu, L., Shu, L.S.** Optimization and Characterization of Laser Cladding of 15-5PH Coating on 20Cr13 Stainless Steel *Journal of Materials Engineering and Performance* 32 (3) 2023: pp. 962 – 977. https://doi.org/10.1007/s11665-022-07157-w
19. **Chen, L.Y., Yu, T.B., Chen, X., Zhao, Y., Guan, C.** Process Optimization, Microstructure and Microhardness of Coaxial Laser Cladding TiC Reinforced Ni-based Composite Coatings *Optics & Laser Technology* 152 2022: pp. 108129. https://doi.org/10.1016/j.optlastec.2022.108129
20. **Saeedi, R., Razavi, R.S., Bakhshi, S.R., Erfanmanesh, M., Bani, A.A.** Optimization and Characterization of Laser Cladding of NiCr and NiCr-TiC Composite Coatings on AISI 420 Stainless Steel *Ceramics International* 47 2021: pp. 4097 – 4110. https://doi.org/10.1016/j.ceramint.2020.09.284
21. **Fu, L.L., Yang, J.S., Li, S., Luo, H., Wu, J.H.** Artificial Neural Network-Based Damage Detection of Composite Material using Laser Ultrasonic Technology *Measurement* 220 2023: pp. 113435. https://doi.org/10.1016/j.measurement.2023.113435
22. **Genna, S., Menna, E., Rubino, G., Trovalusci, F.** Laser Machining of Silicon Carbide: Experimental Analysis and Multiobjective Optimization *Ceramics International* 49 2023: pp. 10682 – 10691. https://doi.org/10.1016/j.ceramint.2022.11.258